Biomed Microdevices (2014) 16:465–478
DOI 10.1007/s10544-014-9849-1

The F-actin and adherence-dependent mechanical differentiation of normal epithelial cells after TGF-β1-induced EMT (tEMT) using a microplate measurement system

T. H. Wu · Y. W. Chiou · W. T. Chiu · M. J. Tang · C. H. Chen · Ming-Long Yeh

Published online: 15 March 2014
© Springer Science+Business Media New York 2014

Abstract The epithelial to mesenchymal transition (EMT) is known to involve several physiological and pathological phenomena. In this study, we utilized a microplate measurement system (MMS) approach based on the deflection of a flexible micro-cantilever to measure cell stiffness (in Pa) and adhesion force (in nN) of a single cell during EMT with nN resolution. Our results demonstrated that after transforming growth factor-β1 (TGF-β1) induced EMT (tEMT), NMuMG cells became stiffer due to thicker and more abundant F-actin and displayed stronger vinculin accumulation after long-term cell-substrate adhesion. The MMS could distinguish differences in compressive stiffness (219±10 and 287±14 Pa), tensile stiffness (114±14 and 132±12 Pa), and adhesion force (150±42 and 192±31 nN) between cells before and after tEMT. However, without proper development of the F-actin structure and adequate adherent time, the mechanical differences were diminished. After tEMT, the cells with increased stiffness and a cell-substrate adhesion force benefited by migrating more rapidly and had more invasiveness. Thus, this technology has the potential to benefit research focused on cancer diagnosis, drug development, and cell-substrate interactions.

Electronic supplementary material The online version of this article (doi:10.1007/s10544-014-9849-1) contains supplementary material, which is available to authorized users.

T. H. Wu · Y. W. Chiou · W. T. Chiu · M.-L. Yeh (✉)
Department of Biomedical Engineering, National Cheng Kung University, No.1 University Road, Tainan City 701, Taiwan
e-mail: mlyeh@mail.ncku.edu.tw

M. J. Tang
Institute of Physiology, National Cheng Kung University, Tainan, Taiwan

C. H. Chen
Department of Rehabilitation, Kaohsiung Municipal Ta-Tung Hospital, Kaohsiung, Taiwan

Keywords Epithelial to mesenchymal transitions (EMT) · Normal marine mammary gland cells (NMuMG) · Transforming growth factor-β1 (TGF-β1) · Atomic force microscopy (AFM) · Cell stiffness · Adhesion force

1 Introduction

Metastasis remains the leading cause of death worldwide (Buergy et al. 2012). The epithelial to mesenchymal transition (EMT), which converts polarized epithelial cells into motile mesenchymal cells and promotes invasive and migratory properties, plays a key role in the early stages of metastasis (Birchmeier 2005; Labelle et al. 2011). Somatic cells that change from one mature phenotype into another exhibit the property of cell plasticity. Recently, stiffness has been recognized as a quick and quantitative measure to differentiate the types of cells (Suresh 2007), such as compressive stiffness of cells might possibly be used to predict the onset of leukostasis (Lam et al. 2008) and tensile stiffness of cells could be used to grade the metastatic potential of tumor cells (Swaminathan et al. 2011). The importance of cell mechanical properties (CMs) to physiology is appreciated, yet how to identify the cells undergoing EMT is needed further elucidation.

Since 1994, transforming growth factor-β1 (TGF-β1) has been known to be an effective EMT inducer for normal mammary epithelial cells (Miettinen et al. 1994). TGF-β1 has the ability to mediate a diverse range of cellular responses including cell proliferation suppression (Zavadil and Bottinger 2005), cytoskeleton rearrangement and phosphorylation (Beach et al. 2011) and the disruption of cell-cell junctions (Mori et al. 2009). In general, after TGF-β1-induced EMT (tEMT), cells obtain a fibroblast-like shape and lose polarity (Mani et al. 2008). By atomic force microscopy (AFM), the elongated morphology, filamentous actin and stiffer characteristics have been proposed on the cells after

tEMT (Thoelking et al. 2010). It has been shown that disruption of actin filaments by cytochalasin D (cyto-D) results in a softening of fibroblasts (Martens and Radmacher 2008; Rotsch and Radmacher 2000). However, there was still lack of evidence demonstrated the influence of cyto-D on CMs alteration during tEMT.

The EMT is considered to be a significant step in the TGF-β1's stimulatory role in tumorigenesis, such as an increase in cell invasiveness and motility (Kabashima et al. 2009; Zavadil et al. 2001). Cancerous or EMT cells are known to accelerate migration when seeded on a softer, grooved pattern of polydimethylsiloxane (PDMS) (Chen et al. 2009; Wu et al. 2013). Most living cells are anchorage dependent and must migrate to the appropriate location to perform their innate functions. Therefore, knowledge of cell-substrate interactions is crucial for understanding many fundamental biological questions and the design of medical devices (Nerem 2003). Importantly, cells must regulate their mechanical properties through integrin-mediated adherence on substrates with EMT processing (Bates et al. 2005). However, limited studies have tested adherence status influence in cells before and after tEMT.

Numerous apparatuses have been used for cell mechanics measurements. The micropipette aspiration system has been used to measure the adhesion force of a single living cell to a particular type of substrate, the modulus of the cell membrane, and the adhesion force between cell-cell interfaces (Chu et al. 2004; Colbert et al. 2010). However, limitations of this system include large cell deformation during testing and influencing cell behavior by trapping cells with a micropipette. Recently, an AFM-based cell mechanics spectroscope, including a tip or tipless cantilever, was extensively investigated. This device can detect either compressive or tensile cellular interactions with another cell or substrate. However, this spectroscope obtains only short-term adherence behavior (i.e., less than an hour) (Buckley et al. 2012; Friedrichs et al. 2010a; Shen et al. 2011; Stewart et al. 2011). It is doubtful that the adherence duration is long enough for cell mechanic measurement.

The dual plate measurement is composed of dual plates or rods placed in parallel (Itabashi et al. 2009; Matsui et al. 2009; Ofek et al. 2009). After applying the proper biochemical surface coating, both stress fiber and single-cell mechanical properties can be measured in suspension or adherent cells. The system used by Mitrossilis et al. was made from micropipette with geometry in rod (Desprat et al. 2006; Mitrossilis et al. 2009, 2010). The cell-plate contact surface therefore is not flat plane. We believe that the geometry will affect the contact area dependent stress or force measurement.

Aforementioned, we endeavored to establish a microplate measurement system (MMS) to investigate whether the cell stiffness and adhesion force were responsive to TGF-β1 induction, and the effect on invasiveness and motility was examined concomitantly. Also, cell mechanical alterations involved in mediation by actin was revealed by adding inhibiting drug, Cyto-D. Eventually, we validated the period, extremely long or short, that cell-ECM adhesion formed before measurement may lead to the applicability of MMS.

2 Materials and methods

2.1 TGF-β1-induced EMT model

Normal murine mammary gland epithelial cells (NMuMG) were selected as a model for tEMT because of their high efficiency for EMT induction by TGF-β1. Cells were maintained in high-glucose Dulbecco's modified Eagle medium (DMEM) supplemented with 10 % fetal bovine serum (FBS) and 10 μg/ml insulin. The cells were grown at 37 °C in a humidified 5 % CO_2 incubator. The cells were trypsinized every 3–4 days following 0.25 % trypsin treatment, and the medium was replaced every 2–3 days. To induce EMT, cells were treated with 10 ng/μl recombinant human TGF-β1 (PeproTech, London, United Kingdom) in 1 % FBS-DMEM for 48 h. NMuMG cells after TGF-β1-induced EMT were defined as the NMuMGemt group.

2.2 Immunofluorescent staining

Immunofluorescence staining was employed to confirm whether TGF-β1 induced the transformation of NMuMG into mesenchymal cells as determined by E-cadherin expression and F-actin arrangements. Anti–E-cadherin and anti-vinculin antibodies from BD Pharmingen (BD Bioscience, California, USA) were conjugated with a goat anti-mouse AlexaFluor 488 secondary antibody (Invitrogen, California, USA). F-actin was stained with rhodamine phalloidin (Cytoskeleton, Denver, USA) and counterstained with Hoechst33258 (ANASPEC, California, USA). The E-cadherin, F-actin, vinculin and nucleus conjugated fluorescence were excited with a laser at 488, 568 or 405 nm, respectively, and detected by a scanning confocal microscope (FV-1000, Olympus, Japan).

2.3 Cell height and spreading area topography scanning by AFM

The atomic force microscope (JPK, NanoWizard II, Germany) was settled up on the inverted microscopy (Zeiss Axio Observer, Germany). Pyramid cantilever (P1L450B, NANOSENSORS, US) with 1 nN-μm-sec^{-1} loading rate in contact mode was utilized to obtain the height and the spreading area of cell. Scanning rate was designed as 1 Hz (200 μm/s). Image J was used to calculate the spreading area of cell.

2.4 Experimental setup of force measurements using MMS

Glass microscope slides were sterilized in 70 % ethanol overnight and exposed to UV irradiation for 15 min. To coat an extracellular substrate layer, the slides were incubated in 10 μg/cm^2 type I collagen from rat tails (BD Bioscience, California, USA) overnight followed by washing in PBS twice. Suspended NMuMG or NMuMGemt cells (2× 10^5 cells/ml) were allowed to adhere to the collagen-coated slides in a 6 cm dish. Meanwhile, the NMuMGemt cells were additionally treated with TGF-β1 for EMT induction. After a 48 h incubation, the cell seeding glass slides were perpendicularly placed in a 10 cm dish. Culture medium containing 30 mM HEPES was added to the dish to prevent pH changes over the course of the experiment. The dish was placed on an inverted microscope (AE31, Motic, China) that was positioned on an anti-vibration table, and all experiments were performed in an incubation chamber at constant temperature with controlled CO_2 levels.

According to the 48 h of adherence period, both cell group almost fulfilled the area of glass slide. However, in terms of single cell mechanic, we choose the isolated cell for measurement. Selected cells were observed using a 40× objective for all experiments. Meanwhile, from adherence aspect, we excluded the cell that early detached from the con-A side but not the expected collagen side, whereas the tensile mechanical properties are not fully measured. To obtain a calibration scale, a standard grid image was taken using the same objective with a CCD camera (TCA-10, Tucsen, China). These images were subsequently examined to obtain a 4.8 pixels/μm calibration constant.

MMS was modified version of previous set-up (Nagayama et al. 2007) to axially compress-relax-retract individual cells captured between a rigid plate and the back-plate of AFM which were oriented horizontally (contrary to the classical vertical orientation) in order to simultaneously observe cells and measure their stiffness. In addition, the commercial product as AFM cantilever overcame the inconvenience of glass microplate reproduction (Mitrossilis et al. 2010). Though prior research has investigated the TGF-β1 effects on the cell in resisting compression, those studies only examined forces applied locally onto the cell (Canetta et al. 2005; Thoelking et al. 2010). However, cells typically experience mechanical forces applied along them entirety (Guilak and Mow 2000). A schematic representation of the experimental geometry and optical phase contrast images are shown in Fig. 1a, b and c.

For calibration, a PDMS substrate of Young's modulus E= 5 kPa was estimated in advance using a material testing system (LRX5K, Lloyd Instrument, England). According to a previous study (Mitrossilis et al. 2010) for simulating this substrate as a spring, in this case, the spring constant of PDMS, k_p, was equal to the relationship between the pulling force, and the elongated deformation was given by Eq. (1):

$$k_p = \frac{EL}{(1-\nu^2)} \tag{1}$$

where L is the length of the cantilever-PDMS contact area and ν is the Poisson's ratio of the substrate (figures s1). The measured L and ν values are ≒ 10 μm and ≒ 0.25, respectively, and Young's modulus, E ≒ 5 kPa, was equivalent to k_p, which was 0.09 μN/μm. The mechanical equivalence between the cantilever and PDMS then implied that

$$k_p\delta_p = k_c\delta_c \tag{2}$$

The tensile force generated by the drag force from cantilever deflection induced tension force onto the PDMS substrate (figures s1). During a cantilever-PDMS separation experiment, we could measure the elongated deformation of PDMS, where (δ_p) was 3 μm and the deflection of cantilever (δ_c) was 30 μm. Therefore, the estimated k_c was 0.009 μN/μm according to Eq. (2), and this was then applied as a spring constant for the standard cantilever. Each flexible cantilever used in our experiments was calibrated with respect to the standard cantilever.

After calibration, all AFM cantilevers were cleaned in sulfochromic acid to remove organic compounds and then were sterilized. The back-plate of AFM cantilevers were functionalized in 0.5 mg/ml concanavalin A (con-A; Sigma, California) for 30 min at room temperature. The 3D position was manually adjusted to near the surface of glass slide and parallel aligned by verifying the microscopy images in a different focus plane than the focus drive.

We used AFM cantilever as force sensing paradigm without the multipart design of AFM. The resolution of MMS was calculated from the deflection and spring constant of cantilever by using minimum unit (1 pixel=0.21 μm) multiplied by the calibrated spring constant (0.009 μN/μm) of the cantilever. Therefore, the estimated resolution was 2 nN.

A complete set of mechanical measurements were divided into four stages, and the compression and tensile experiments were shown in video (supplementary video 1 and 2). In the first stage (1: compression), using a piezoelectric actuator, the con-A coated flexible cantilever was displaced by a prescribed amount (typically 5 μm) at a constant speed (0.42 μm/s), and the cell was compressed by the cantilever, resulting in displacement (defined as negative) of the cantilever deformation of the cell. In the second stage (2: relaxation), the cantilever was held in this position for 180 s to ensure the occurrence of con-A attachment and to observe the force relaxation behavior during which time the cell relaxed as it accommodated the imposed deformation (note the small decrease in the magnitude of the force during the relaxation stage). Between the third (3: recovery) and fourth stages (4: tension) of the experiment, the cell adopted two different status with a transition occurring

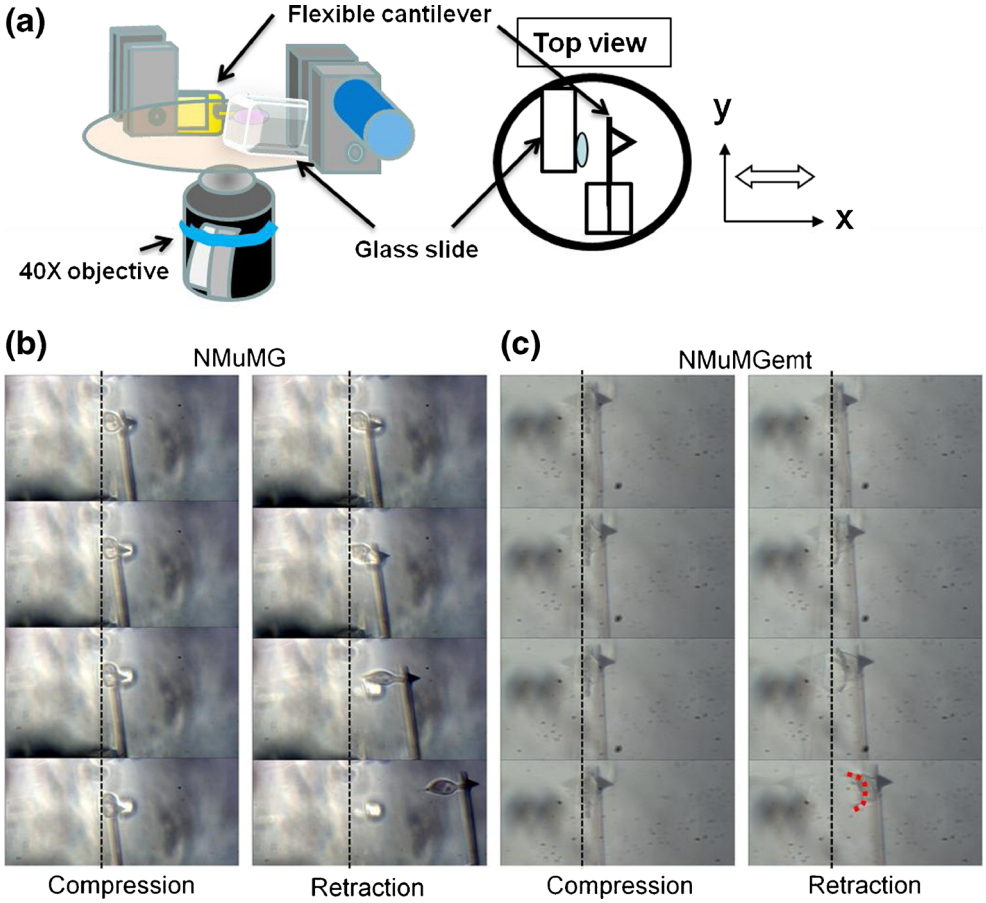

Fig. 1 **a** Schematic drawings of the MMS setup. A cell is placed between glass slide and the back-plate of AFM cantilever symmetrically mounted on each side of the microscope stage. The Cartesian coordinate axes of the images are defined by the indicated plot, and the flexible cantilever is driven along the X-axis by a stepper motor. **b** Representative phase contrast images of NMuMG cells undergoing mechanical measurements. The dotted line represents the edge of the glass slide, where the measured cell adhered. **c** Representative phase contrast images of NMuMGemt cells. The *dotted curve* in *red* indicates the speculated end-reinforced adhesion of NMuMGemt during retraction

when the contact patch decreased upon ascending into a plateau, and the steep slope of stress-strain curve became slack. In the third and fourth stages, the cantilever was pulled the cell away from collagen coated glass slide, which brought the cantilever back to its original position (zero force). The maximum adhesion force may be directly measured during this pull-off period. We noted that the same numbering scheme for different stages was used throughout this article.

Additionally, we executed detachment assay by modified MMS according to the previous set-up (Wu et al. 2005). To decouple the effort of cell-ECM adherence from the self-contractility synchronization, we did the detachment assay by modified MMS. Take a 90° turn of the cantilever position, meanwhile, the perpendicular position between glass-slide and cantilever was located. Start with the back-plate of cantilever approached to the target cell, which was detached with constant velocity (0.42 μm/s) and the deflection of cantilever was measured by image analysis process.

2.5 Image analysis and mechanical properties estimation

Each cell was recognized as either a spheroid or hemi-spheroid with rotational symmetry around the x-axis. The x- and y-dimensions were defined as the cell height and diameter, respectively. Axial strain (ε) was calculated as a change in cell height (measured immediately) divided by the initial cell height (measured prior to compression). In addition, the contact area (A_c) between cells and the cantilever was assumed to be circular because of the symmetry between the cell shape, and its value was estimated from the measured cell diameter, which changed progressively during measurement. The deflection of the calibrated cantilever was measured by synchronizing images. The measured force (F) was calculated by using Hooke's law from the deflection of cantilever multiplied by the calibrated spring constant of the cantilever. An image analysis program was encoded using the MATLAB software (Math Works) with the following steps: mean filtering, histogram equalization, edge filtering, edge detection, and force reduction as performed in a previous study (Wu et al. 2005) to detect the cantilever deflection pixels and transform them into a force measurement. Stress (σ) was calculated using Eq. (3):

$$\sigma = \frac{F}{A_c} \tag{3}$$

Stiffness (E) was estimated from the stress versus the strain using Eq. (4):

$$\mathrm{E} = \frac{\sigma}{\varepsilon}. \tag{4}$$

2.6 Ibidi wound healing assay

Besides inducing the phenotypic characteristics of EMT, TGF-β1 treatment of NMuMG cells also results in behavioral changes that are associated with EMT and are important aspects of TGF-β1's stimulatory role in tumorigenesis, such as an increase in cell motility and invasion. We first examined the effect of the increased motility of cells in response to TGF-β using the monolayer wound assay (Lee et al. 2011). Thus, NMuMG cells were treated with or without TGF-β in the medium for 48 h, at which time all TGF-β–treated cells had undergone EMT. To measure cell migration, confluent NMuMG control and tEMT cells kept in serum-free medium for 24 h were wounded with a μ-Dish 35-mm culture ware (ibidi GmbH, integrated BioDIagnostic). After washing, the medium was replaced by normal culture medium. Photographs of the wounded area were taken every 3 h by phase–contrast microscope. For evaluation of wound closure, four randomly selected points along each wound were marked and the horizontal distance of migrating cells from the initial wound was measured with Image J (version 6.0; NIH).

2.7 Transwell invasion assay

Cells were allowed to migrate across a 8 μm pored membrane (BD Biosciences, California, USA) towards a medium containing 10 μg/mL FBS at 37 °C as previously described (Albini et al. 1987). Briefly, we first placed inserts into a 24-well plate. Then, 50 μl of collagen matrigel (BD Biosciences), which was diluted to 1 mg/ml, was added to the inserts with a membrane. Next, we added 600 μl of DMEM containing 10 % FBS and 200 μl of prepared cells (4×10^4/ml) in DMEM containing 1 % FBS to the insert. After a 48 h incubation, the cells on the membrane were fixed and stained with methanol and Giemsa, respectively, and the cells were counted under 20× objective.

2.8 F-actin polymerization inhibiting by Cytochalasin D

To elucidate the contribution of F-actin to the tEMT effects on cell mechanics, 10 μM cytochalasin D (cyto-D; Sigma, California, USA), an F-actin polymerization inhibitor, was used to disrupt the F-actin filaments of cells in 60-mm dishes for 1 h. Subsequently, the cyto-D treating cells mechanics were measured by MMS and the F-actin inhibition by cyto-D was revealed by immunofluorescent staining.

2.9 3 min adherence cell mechanical measurement experiment

According to the AFM based single cell force spectroscopy (AFM-SCFS) experiment preparation, whereas they harvest cells by incubation with 1.5 ml 0.5 % trypsin-EDTA for about 2 min (Friedrichs et al. 2007, 2010a, b, 2012, 2013a, b). However, previous result showed that low trypsin concentrations produced faster spreading, a higher number of intact integrins, and rapid focal adhesion formation (Brown et al. 2007). Therefore, we suspended cells by treating 0.25 % trypsin for 5 min and the appropriate neutralization solution was added, the cell suspension was immediately centrifuged, resuspended in culture medium, and then used in 3 min adherence experiments. We used a con-A coated cantilever to bind single suspended cells as described by previous methods using AFM (Friedrichs et al. 2010a, b). After attaching the cell to the cantilever, so called cell probe, allow the cell to recover for 5 min. During this time, the cell will form firm contacts with the cantilever surface (Friedrichs et al. 2010a, 2013a). Otherwise, the possibly effective low dose and long duration trypsin for cell suspension, as long as the recovery time was enough for a living cell rebuild their adherent molecules on the membrane.

On the cell-adhered side of the glass slide, collagen, which is the most abundant ECM in the human body, was selected as a substrate coating in this study. Because a passive and non-physiological connection existed between con-A and cell membrane receptors (Friedrichs et al. 2010a), there was no adhered protein competition between con-A and collagen-coated substrates. This experiment was suitable for elucidating whether the 3 min adherence time was sufficient for generating tEMT-induced mechanical alterations. After properly set-up, the cell probe was driven toward glass slide as compressive experiment, then drag backward as tensile experiment. The applicability was revealed in an AFM-SCFS experiment, the initially applied contact force will probably help to displace the pericellular coat to facilitate receptor–ligand interactions, which explains, why receptor-mediated cellular adhesion can be established within few seconds (Taubenberger et al. 2014).

2.10 Data analysis

Statistical analyses were performed using SPSS version 17.0 software. A normal distribution was first verified using a Shapiro-Wilk test. The Student's *t*-test was used to examine differences between groups.

3 Results and discussion

3.1 Differentiation the effect of tEMT on NMuMG cell morphology, F-actin, E-cadherine and vinculin arrangement, and cell height and spreading area

The alignment of intracellular components and membrane molecules plays a decisive role in determining the cell mechanical properties during the cascade of cell attachment and growth (Li et al. 2003). In this study, after tEMT, NMuMGemt

cells acquired an elongated, fibroblast-like shape and altered the F-actin, vinculin and E-cadherin arrangement.

Using E-cadherin fluorescent staining, we further confirmed that the NMuMGemt cells underwent a complete induction of tEMT. E-cadherin primarily accumulated at the cell-cell junction sites of NMuMG cells (Fig. 2a). In contrast, upon the TGF-β1 induction of NMuMGemt cells, E-cadherin was cleaved from the outer membrane and then endocytosed from the membrane into the cytoplasm in a granular pattern for further degradation (Fig. 2b). During cell adhesion, vinculin was recruited from the cytoplasm to the focal adhesion complex, and it was more concentrated and abundant in NMuMGemt than NMuMG cells (Fig. 2). In addition, the F-actin distribution network in the NMuMGemt cells had assembled into bundles across the nucleus, formed actin-cap, after tEMT. Additionally, F-actin-vinculin colocalization was more prominent in NMuMGemt cells (Fig. 2b).

In comparison with the morphology of cells before and after cyto-D treatment, the images demonstrated that spreading NMuMG and NMuMGemt cells shrank and reduced in size due to cyto-D inhibition. The F-actin depolymerized as granular monomers, and decreased the colocalization with vinculin after treatment with cyto-D for 1 h (Fig. 2). Here we identify a small subset of F-actin in the NMuMGemt cells formed actin cap, a highly ordered filamentous actin structure that is anchored to the top of the nucleus. Actin cap associated focal adhesions as major mediators of cellular mechanosensing and a critical element of the physical pathway that transduce mechanical cues all the way to the nucleus, by its specific function regulated by actomyosin contractility (Kim et al. 2012).

In comparison of vinculin distribution, it was sparsely located at NMuMG cells cortex, and it was dotted and condenser in NMuMGemt cells. After cyto-D inhibition, the vinculin was reduced in size and numbers (Fig. 2). These findings led us to assume the switch of the role for vinculin from the regulation of cell-extracellular matrix adhesion to that of actin fibers and suggest the involvement of vinculin in tEMT. Cell adhesion depends on the activity of focal adhesion component and cytoskeleton. Furthermore, the focal adherence protein vinculin played an important role in mechanical signal transduction, focal adhesion formation and intracellular connections with the cytoskeleton.

By AFM, we quantified the cell height and spreading area of the NMuMG and the NMuMGemt cells. After tEMT, the cell height significantly decreased from 8.1±0.4 to 4.5±0.2 μm (Fig. 3a, b, c and d), and the spreading area significantly increased from 1,041.0±67.2 to 1,996.1±179.5 μm^2 (Fig. 3e). In line with the typical cell heights ranged from 7 to 13 μm, depending on size and shape (Fuhrmann et al. 2011). From the AFM scanning images, we distinguished the distinct, rounded-up NMuMG cells, and the flattened-elongated NMuMGemt cells. As the deflection images shown, the NMuMGemt cells demonstrated rippled surface topography revealed the stress fibers formation underneath the cell membrane, actin-cap, after tEMT (Fig. 3c). In comparison with the rounded NMuMG cells, the flattened spreading NMuMGemt cells were stretched out, resulting in reinforced cell pre-stress and nuclear stiffness.

The NMuMG cell height and spreading area were altered by an 80 % decrease and a 90 % increase, respectively, after tEMT. Several groups have worked towards understanding how cell height and spreading area impact measurements of cell stiffness using AFM (Solon et al. 2007; Vichare et al. 2012b). Taken together, these results demonstrate the

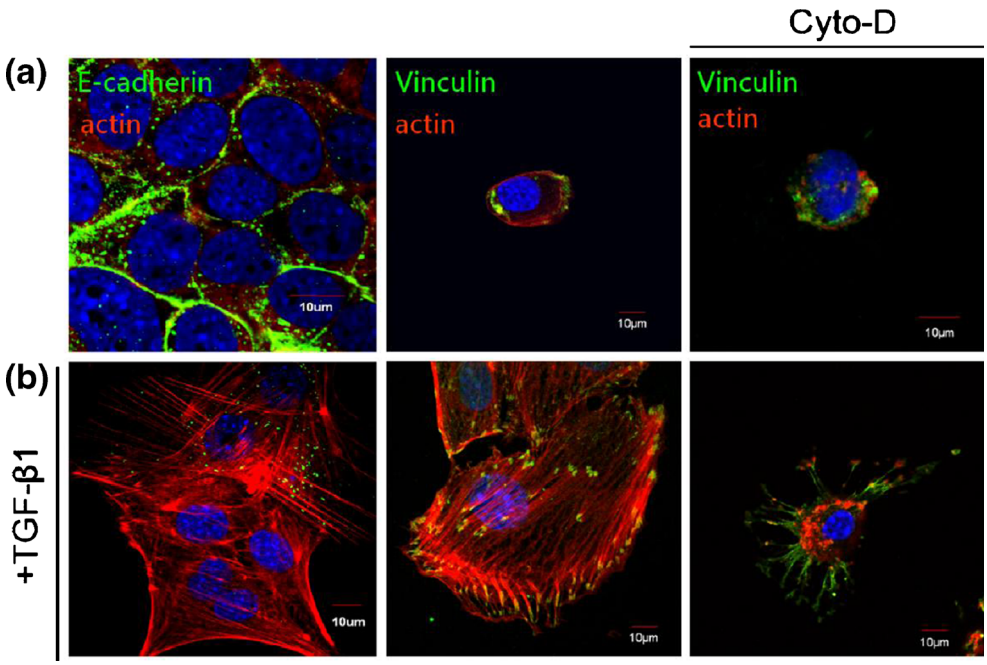

Fig. 2 **a** NMuMG and **b** NMuMGemt cells are immunofluorescent stained with nucleus (*blue*), F-actin (*red*) and E-cadherin or vinculin (*green*). The last column was the immunofluorescent images of cells after Cyto-D treatment. Scale bar is 10 μm

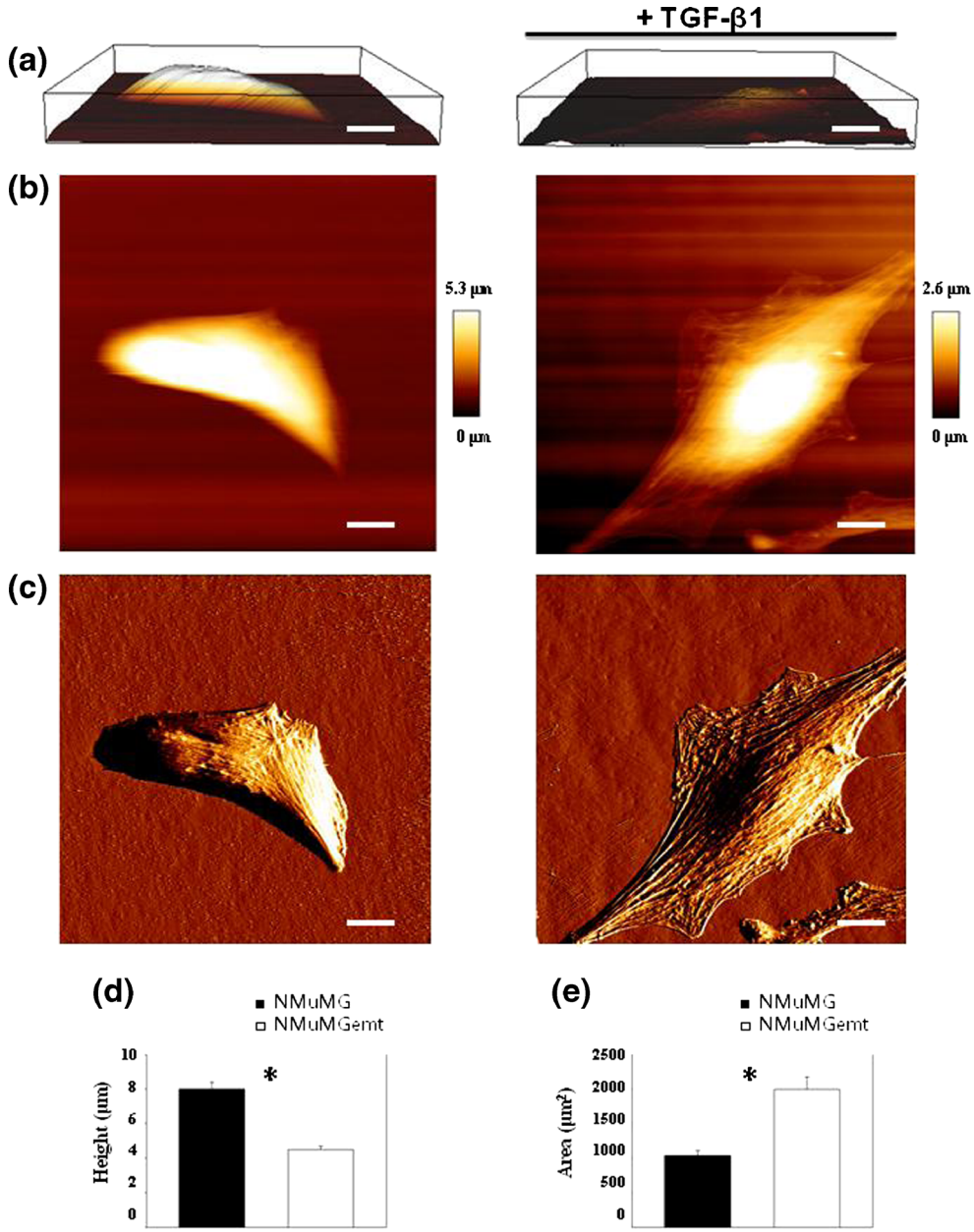

Fig. 3 AFM **a** 3-D reconstructed, **b** height and **c** deflection image of a living NMuMG and NMuMGemt cells. The height of the cell is expressed in color scale 0 (dark fields)—5.3 µm (light fields). **d** and **e** The cell height and spreading area of control and tEMT cells (*$p<0.05$)

significant influence of cell geometry on the cell stiffness, which increased with spreading area (Solon et al. 2007) and decreased with cell height (Vichare et al. 2012b). While the above results illustrate the influence of cell geometry on cell compressive stiffness measurements, the effect of cellular contractility, such as tensile stiffness and adhesion force, were not taken into consideration.

3.2 Mechanical differentiation the NMuMG and NMuMGemt cells

Totally, 23 NMuMG and 25 NMuMGemt cells are measured by MMS. The representative stress-strain NMuMG and NMuMGemt cell curves are shown in Fig. 4a. In the first stage of the experiment (compression (stage 1)), a cantilever push on the cell and glass slide with a force we defined as negative compressed the cell. The compressive stiffness difference obtained between the pre- and post-tEMT cells was 68.2 Pa (i.e., a 31 % increase after tEMT).

Theoretically, cells with softer stiffness under constant compressive loading should have higher compliance. Our compression results consistently demonstrated that untreated NMuMG cells were softer than NMuMGemt cells. In addition, the gross observed cell height and spreading area identified by AFM demonstrated cell type dependent differences. The lower height and wider spreading area were characteristic

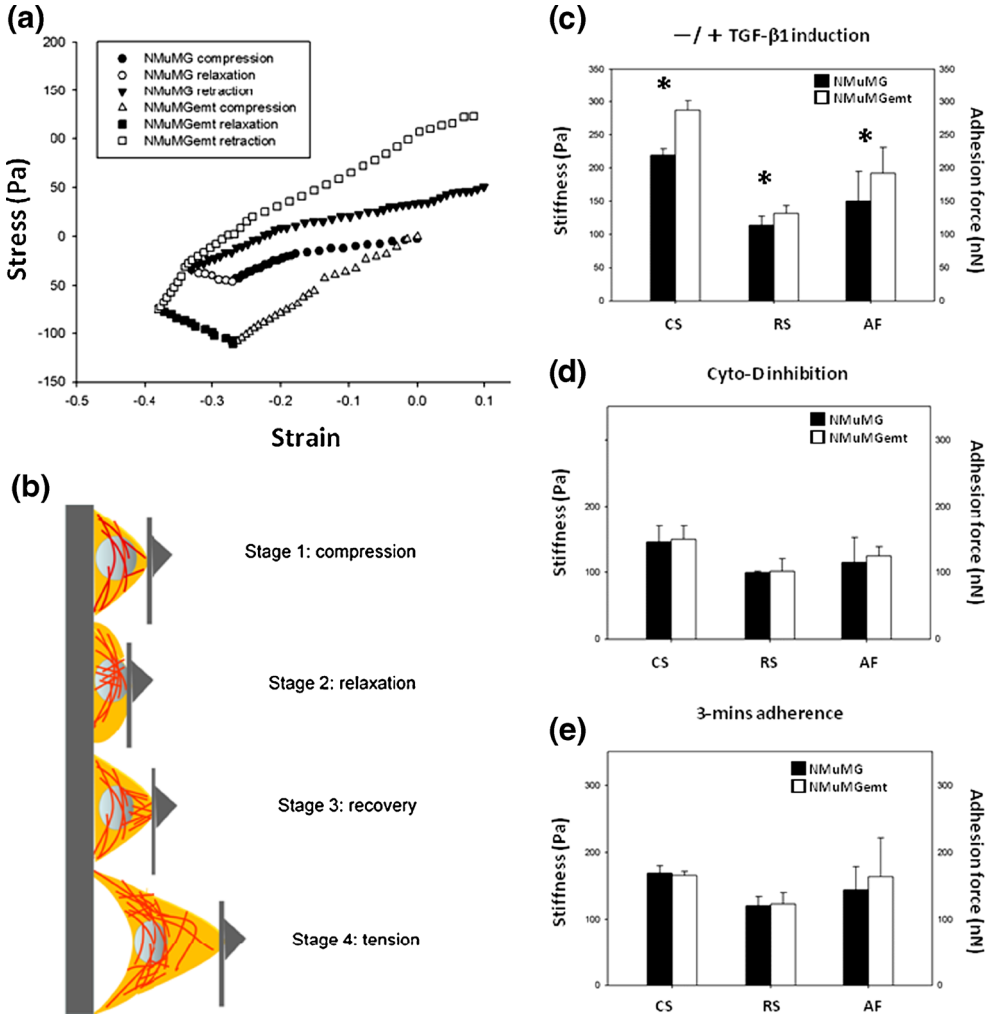

Fig. 4 **a** The stress-strain curves during compression-relaxation-retraction experiment show the different shape between NMuMG and NMuMGemt cells. **b** Schematic drawings of the separated four stages of mechanical measurement. **c** The measured stiffness and cell-substrate adhesion force of both cell types (*$p<0.05$). **d** The effects of Cyto-D treatment on the identified different mechanical properties of NMuMG and NMuMGemt cells. **e** The effects of only 3 min adherence time on the identified different mechanical properties of NMuMG and NMuMGemt cells

of cells after tEMT. In addition, the morphology also contributed to elevated whole cell stiffness and highlights the importance of cell geometry on cell stiffness measurements. Also, Fig. 3e demonstrates NMuMG cells comprising less well-defined filamentous structures that appear as disorganized ridges, while Fig. 3f demonstrates NMuMGemt cells with well-aligned filamentous structures underneath the cell membrane, whereas the most energy were taken under compression (Colbert et al. 2010). This may explain why NMuMGemt cells had higher compressive stiffness than NMuMG cells.

In the second stage of the experiment (relaxation (stage 2)), with constant displacement of cantilever, allowing the cell to relax under the imposed stress. This relaxation stage was also perhaps most intriguing. During this time, the motion of the cantilever correlated with the cell deformation and therefore the force applied. Meanwhile, the relaxation process also allowed a non-specific attachment between the cell membrane and the cantilever. The elastic characteristics of the cell were then dramatically altered by the attachment: the area of the cell-collagen adhesion became wider, and the sandwiched cell transformed from a hemispheric to a spheroid shape.

During tensile experiment, the cantilever attached to cell membrane was pulled. It was divided into stages 3 and 4, the cell shape recovered (stage 3) followed by tethering, and then, it detached from the substrate (stage 4). Initially, the force measure by MMS is dominated by the stretching of the membrane and the cytoskeleton during stage 3. In this stage, cells adhered to the collagen surface must exert forces across their cell body to contract and pull itself. The maximum adhesion force appeared between the actin filaments deboned from the inner-side of membrane at stage 3. This adherence-dependent mechanical difference was correlated with the actin binding to the strong adhesion sites on its membrane. Concomitantly, the other end of the binding actin is anchored to an intra-cellular organ or a particular protein on the nuclear membrane such as Nesprin (Starr and Han 2003; Wang et al. 2009). Under this tightened condition by an intra-cellular generated force, either actin or the nucleus was under "preloading" stress (Vichare et al. 2012a).

According to the works have already been dedicated to the effect of TGF-β1 on cell mechanical properties by Chen et al and Tseng et al (Chen et al. 2007; Tseng et al. 2011), the

contractile forces exerted by adherent cells are typically studied for cells on a 2-dimensional soft substrate, where the deformation of the substrate or structures patterned on the substrate can be used to determine the force. In these cases, the adhesions to the surface are all on the basal surface of the cell, so the contractile forces are all parallel to the adhesions, whereas our measurement have revealed the cell-ECM adhesion force from the vertical aspect. Taken together, we can measure the combined effects of the cell-ECM adhesion and self-contraction forces.

The combined effects of the strong adhesion and self-contraction forces did make the cells after tEMT have more resistance to the traction force. The measured tensile stiffness and adhesion force of the NMuMGemt cells were a reasonable 1.16 and 1.28 times of NMuMG, respectively. Moreover, we have found the difference of adhesion force between control and tEMT cells is 42 nN. We are satisfied with the resolution of MMS (2 nN). It is enough to distinguish the whole cell mechanics. Fletcher et al. had revealed a high resolution AFM combined side-view microscopy with resolution in pN for small force detection (Chaudhuri et al. 2009). From the biological aspect, most cells are response to environment wholly. It is also important to measure bulk cell as a whole. Therefore, our design is more suitable for large amount of whole cell measurement.

At stage 4, the tethered cell was continually pulling, resulting in a decrease in the contact area, and the cell gradually detached from the collagen adhered side through tethering. These linear experimental data are shown in Fig. 4a. In addition, schematic drawings of the cell membrane, cytoskeleton and nucleus during compression (stage 1), relaxation (stage 2), recovery (stage 3) and tension (stage 4) are shown in Fig. 4b.

In this study, cells remained attached to the con-A coated cantilever after each analyzed retraction experiment. This indicated that the cells were tearing from the collagen-adhered side; therefore, the measured retracted mechanics were related to the cell-surface adhesion behavior. The retraction is mediated by a reversible, noncovalent interaction between cell membrane receptor molecules and complementary ligand proteins in the extracellular matrix or synthetic biomaterials through integrin (Saterbak and Lauffenburger 1996). Furthermore, the focal adherence protein vinculin played an important role in mechanical signal transduction, focal adhesion formation and intra-cellular connections with the cytoskeleton. In comparison, confocal images revealed that the vinculin and F-actin colocalization in NMuMG cells was cortically distributed but denser, and filaments were featured in locations in the NMuMGemt cells. During the tEMT process, vinculin was endocytosed inward and then relocalized and accumulated to perform specific cell-substrate adhesions (Turner et al. 1990) such as the abundant gathering of vinculin at the narrowest ends of cells that acquired a spindle-like shape after tEMT. Subsequently, the particular vinculin distribution of NMuMGemt cells resulted in specific new-moon shape tethering during retraction i.e., NMuMGemt cells detached from the center firstly and both ends of the cell margin (Fig. 1c). In contrast, the focal-concentrated phenomenon was not observed for NMuMG cells during retraction. Similarly, upon traction force microscopy, the increased traction force of cells after EMT was speculated and reinforced at the narrowest ends (Chen et al. 2007).

In summary, our experiments measured the cell compliance, contractile behavior and adhesion force applied on a single cell between opposing sides of the cell body and in the normal direction of the attachment surface. MMS enabled the evaluation tEMT effects on cell stiffness and adhesion force. A plethora of cell mechanics approaches have been used to examine differences in the mechanical properties of diverse cell types. We obtained measurements for compressive stiffness (219±10 and 287±14 Pa), tensile stiffness (114±14 and 132±12 Pa), and adhesion force (150±42 and 192±31 nN) for NMuMG cells after tEMT (Table 1, Fig. 4c). Our results were within a measurable range and comparable with results from other studies (Colbert et al. 2010; Docheva et al. 2010; Lee et al. 1994; Thoelking et al. 2010; Thoumine et al. 1996; Wu et al. 2005) despite the fact that the cell stiffness and adhesion force were varied with different measurements including the local point and bulk aspect of the cell. For example, the AFM system was used to measure the local stiffness of PC3 (3–4.5 kPa) and LNCaP (<2 kPa) cancer cells and the proximal kidney tubule epithelium NRK52E cells (1~100 kPa) (Docheva et al. 2010; Thoelking et al. 2010). With regards to the micropipette measurement system, the compressive to tensile modulus of the cells ranged from 55 to 1.3 kPa (Colbert et al. 2010). Moreover, the cell adhesion force have reported values ranging from 20 to 961.0 nN (Lee et al. 1994; Thoumine et al. 1996; Wu et al. 2005). Modified from the previously developed one (Wu et al. 2005), by turning the cell-plate and cantilever from horizontal to perpendicular to the stage of microscope, and we can execute detachment assay (figure s2, Table 1), whereas the application in biomaterial development is available. However, the perpendicular detachment force was not significantly different between cells before and after tEMT. Contrary, the horizontally measured adhesion force demonstrated the synchronized effort of cell adherence and self-contractility, and revealed the 28 % significant elevation after tEMT. Reasonably, we prefer the adhesion force measured by typical MMS, rather than the detachment force measured by the detachment experiment. Noticeably, the importance is that increased contractility resulted in the higher adhesion force and reinforced the adherent mechanical properties after tEMT.

From the statistical power examination aspect, MMS was able to significantly distinguish the tEMT phenotype with fewer cells than those required for other techniques. The

Table 1 The overall cell mechanical properties and functional behaviors of NMuMG and NMuMGemt and the effects following Cyto-D inhibition and 3-min adherence experiments

	48 h culture	Cyto-D inhibition	3-min adherence
NMuMG	(total, n=23)	(total, n=22)	(total, n=20)
Compressive stiffness (Pa)	219±10[a,b,c]	146±24	169±11[b]
Tensile stiffness (Pa)	114±14[a,b]	99±2	121±10[b]
Adhesion force (nN)	150±42[a,b]	110±31	142±34[b]
Detachment force (nN)	85±21		
Wound closure rate	44 %[a]		
Invasion count (per 4×10^4 μm^2)	42.2±1.1[a]		
Cell height (μm)	8.1±2.5[a]		
Spreading area (μm^2)	1,041.0±329.3[a]		
NMuMGemt	(total, n=25)	(total, n=21)	(total, n=20)
Compressive stiffness (Pa)	287±14[b,c]	149±20	166±6[b]
Tensile stiffness (Pa)	132±12[b,c]	101±20	123±17[b]
Adhesion force (nN)	192±31[b,c]	121±13	160±51[b]
Detachment force (nN)	92±28		
Wound closure rate	96 %		
Invasion count (per 4×10^4 μm^2)	53.3±2.2		
Cell height (μm)	4.5±1.1		
Spreading area (μm^2)	1,996.1±718.1		

α=0.05

[a] Significantly different from NMuMGemt

[b] Significantly different from cells with Cyto-D inhibition

[c] Significantly different from cells adhered for 3 min adherence

difference between groups and variation within each group play an important role for sample size determination. To determine the appropriate number of cells to measure, one needs to take into account the variations in the population cells. However, we measured a relatively smaller amount cells (for cell mechanics n=20–25; for cell migration n=23–34) with acceptable group variation (from 4 to 22 %).

In comparison, the measured cell counts of previous studies used dual plate measurement apparatus (n=8–60) (Colbert et al. 2010; Mitrossilis et al. 2010; Nagayama et al. 2007; Ofek et al. 2009) were less than those used AFM as measurement tool (n=60–177) (Buckley et al. 2012; Cross et al. 2008, 2011). Subsequently, the stiffness measured by microplates had less variation (from 8 to 24 %) (Colbert et al. 2010; Mitrossilis et al. 2010; Nagayama et al. 2007; Ofek et al. 2009), but results from AFM measurement showed a wider variation (from 13 to 75 %) (Buckley et al. 2012; Cross et al. 2008, 2011) (Supplementary Table 1). Therefore, due to locally detection aspect, more cells were needed to overwhelm the innate variation of measurement by AFM (Lekka and Laidler 2009).

3.3 The effect of tEMT on cell migration and invasion behaviors

To measure cell migration, equal numbers (1×10^4) of control and tEMT cells were seeded in the ibidi wound healing chambers. After 24 h observation, cells that had been treated with TGF-β1 and had undergone EMT showed a 96 % wound closure. In contrast, cells that were not treated with TGF-β1 had maintained their epithelial phenotype showed a 44 % wound closure. Exposure to TGF-β1 treatment elevated the wound closure of cells that had undergone EMT from 44 to 96 % (Table 1, Fig. 5a and c).

After 48 h, cells that underwent tEMT significantly invaded through the membrane (Table 1, Fig. 5b and d). In a matrigel invasion assay performed on collagen matrigel-coated inserts, the transmitted cell number was significantly increased (1.26 times) after tEMT even though the cell invasion activity may be highly dependent on cytokine stimulation, such as that of TGF-β1, as had been proposed previously (Kabashima et al. 2009). In terms of oncology, alterations in the mechanics after tEMT are critical for metastasis. Before invasion, cancer cells require a dramatic reorganization of the cytoskeleton and remodel the cell-matrix adhesive site, which is initiated by an integrin-mediated adhesion switch (Giampieri et al. 2009). These cells gain the ability to invade into the surrounding tissue and bear higher stress (Buckley et al. 2012). From a cell mechanic aspect, in a mock 3D microenvironment, the most distal front end of the cell perpendicularly crossed the coating layer through porous inserts and then latched onto the opposite side of the substrate. Meanwhile, the strong intracellular traction forces could drag the following cell body entirely across. In addition, the higher stiffness of cell could endure the dramatic deformation during cells transmission. The cells were reasonably more prepared to invade the 3D environment after tEMT.

3.4 Cyto-D inhibited actin affect cell mechanical properties

Totally, 22 NMuMG and 21 NMuMGemt cells are measured by MMS. After cyto-D treatment, the NMuMG and

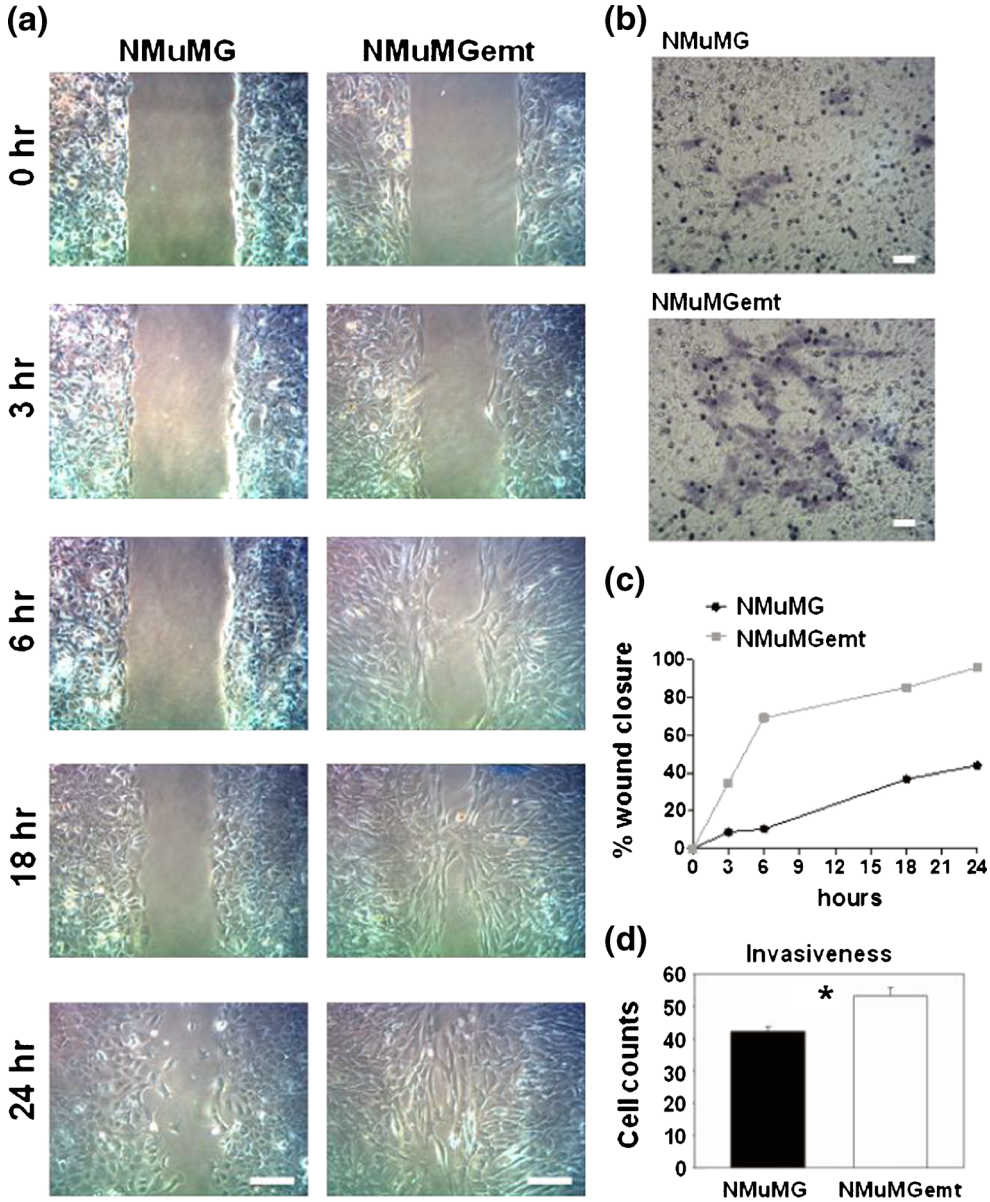

Fig. 5 Effect on migration and invasion of NMuMG cells after TGF-β–induced EMT. **a** The migration of the cell monolayer was observed by time-lapse microscopy and photography every 3 h for 24 h after wounding. Original magnification was 10×. **b** NMuMG and NMuMGemt cells were plated in the transwell chambers for 48 h. Cells invading the matrigel-coated membrane were stained with Giemsa and counted. **c** The percentage of wound healing was calculated from the mean of four wound widths at each time point. **d** The bar-plots showed significant increases in the number of invading cells after tEMT (*$p<0.05$). Scale bar, 50 μm

NMuMGemt cells underwent significant shape shrinkage, and the F-actin network was no longer maintained. In addition, we found that the compressive stiffness, tensile stiffness and adhesion force of both the NMuMG and NMuMGemt cells was significantly decreased after cyto-D treatment (Table 1, Fig. 4d).

The decreased adhesion force that occurred with the suppression of the actin network by cyto-D has been shown to reduce or completely abolish the cell contractility across different cell types and geometries (Sen and Kumar 2009). Cell softening observed under this drug treatment highlights the direct contribution of cell contractility to cell stiffness measurements.

There were 40 % of data excluded from the tensile experiment executed on cyto-D treated cells. As we known, the cell-con-A connection was through the covalent binding with glycoprotein on cell membrane. In addition, we had found that the cytoskeleton-membrane connection was relatively important when cell under tension. Without well connected structure, the drag force from con-A coated cantilever could not transport toward the cell-collagen adhesion sites. Subsequently, the cells wrinkled after cyto-D treatment, decrease the available glycoprotein site on cell membrane. It will result in the cell early detached from the con-A side but not the expected collagen side, whereas the adhesion force is extremely low.

In contrast, no more than 5 % of data had been exclude among cells without cyto-D treatment. These cells are supposed to be strong adherence group with high adhesion force, and the drag force from con-A passive attachment is not sufficient to detach cell from collagen side.

This study validated the actin and focal adhesion contribution to the cell mechanics generated by cyto-D inhibition. We attempted to confirm whether mature actin-membrane adhesion site connections contribute to mechanical alterations in the tEMT. After cyto-D treatment, the dynamic cell morphology adaptation disappeared due to the inhibition of F-actin assembly and depression of the self-contractile forces at the adhesion sites via connections with the myosin light chain (Stewart et al. 2011). Consequently, the mechanical differences between the two cell types was diminished. In sum, cyto-D treatment eliminated TGF-β1-induced cell mechanical changes. Our data suggest that mechanochemical regulation may not be the only mechanism of cell adaptation to their mechanical environment. In some sense, cells can feel with their mechanical sensors, such as the integrin-dependent adherence pathway. Within this pathway, the inhibition of actin formation by cyto-D induction affects the architecture of the cell structure for mechanical property development.

3.5 In 3 min adherence time affect cell mechanical properties

In addition, experiments were performed to assess the effects of only 3 min adherence on the mechanical property alterations of NMuMG cells after tEMT. Totally, 20 NMuMG and 20 NMuMGemt cells are measured by MMS. None of the mechanical properties for both control and tEMT cells demonstrated differences due to immature cell membrane-ECM connections (Table 1, Fig. 4e). The trypsinized floating cells were under a micro-trauma state, and the membrane adherence proteins needed time to recover. It took 5 min to prepare and drive the cantilever attached cells onto collagen-coated glass slides. Consequently, during a 3 min relaxation (stage 2), the adherence between cells and the ECM was not completely developed. However, trypsin detached cells had a much lower adhesion than the EDTA detached cells, somewhat lower for 0.025 % trypsin-EDTA detached cells, and lowest on 0.25 % trypsin-EDTA detached cells (Wang and Cooper 2012). Therefore, the relevance of our experiment was limited as the lower adherent property we measured. To obtain more convincing data, future studies should apply EDTA or other non-proteolytic method for cell suspension.

It is well known that adherent cells are under pre-stress and exert contractile traction forces on their underlying substrates as a part of mechanical sensing substrate properties (Engler et al. 2006; Wang et al. 2002). It has been postulated that cell adhesion involves a two-step process comprising initial integrin-ligand binding followed by rapid strengthening. In 2007, Taubenberger et al. measured the detachment force of Chinese hamster ovary cells on glass slides coated with collagen. These authors found that cell adhesion increased slowly during the first 60 s, and forces associated with the smallest rupture events were consistent with the breakage of individual integrin-collagen bonds. After a 60 s contact duration, a fraction of the cells rapidly switched into an activated adhesion state by up to a 10-fold force increase. The cells achieved stable bonding after a 180 s contact duration (Taubenberger et al. 2007). Based on only a 3 min cell-ECM contact period in this study, we assumed that the non-differentiated mechanical properties of both cell types were in the initial binding phase without strengthening.

However, the stiffer and higher adhering properties of NMuMGemt cells needed a longer adhesion time for establishment. The strengthening response arises from increases in the cell–substrate contact area (spreading), receptor recruitment to anchoring sites (clustering), and interactions with cytoskeletal elements that lead to enhanced force distribution among bound receptors via local membrane stiffening (focal adhesion assembly) (Lotz et al. 1989). In a study by Gallant et al., the adhesion force between fibroblasts and a fibronectin-coated substrate initially rapidly increased and achieved a steady state after 4 h. This result also supports the adhesion strengthening hypothesis (Gallant et al. 2005). When compared with the this study, the cell adhesion force after a 48 h adherence was higher than that of the 3-min contact adherence by 18 % (Table 1, Fig. 4e).

We elucidated the speculated mechanical characteristics dependent on cell-ECM adhesion formation. This formation may synergistically act with the mechanosensitivity of focal contacts. For instance, actin-dependent sensitivity may adapt cytoskeletal tension on the whole-cell scale, and this tension will then be transduced locally—through focal contacts sensitivity—into adhesion complexes of an adapted size and stability. Such a synergistic scenario may explain how local activity at the focal contacts can be coordinated on the whole-cell scale. With regards to the absence of differences in the stiffness results demonstrated for the 3-min adhesion, the immature binding environment was not suitable for differentiating cellular phenotypes by the mechanical alteration of cells after tEMT by MMS. Several advantages were achieved in this design of MMS. Firstly, our design propose a parallel dual plate was more suitable for measurement. In contrast, the microplate used by Mitrossilis et al. was made from micropipette with geometry in rod (Mitrossilis et al. 2010). The cell-plate contact surface is not an flatten plane. It will affect the contact area dependent stress or force measurement. Second, we calibrated the spring constant of cantilever *in-situ* where experiment taken place. The third, we seeded cells on the collagen coated glass plate long enough for physiological process undergoing. In terms of adherence status, our findings suggest that the cell mechanical alteration after tEMT takes time to occur.

4 Conclusion

This study used a self-built MMS to obtain higher adhesion forces (28 %) and stiffer (31 % for compressive and 16 % for

tensile stiffness) mechanical properties after cells shifted toward the mesenchymal type through tEMT. In terms of clinical applications, cell stiffness differences can be measured by AFM (Cross et al. 2008, 2011) and then used to further differentiate between the malignant stages of leukemia (Lam et al. 2008). In the future, MMS could be developed to identify changes in the mechanical properties of several cell types in minutes with nN resolution. A cell discrimination platform or strategy for inhibiting cancer cell EMT progression by targeting their mechanical properties before and after the transition may be developed. Consequently, this study also observed that alterations existed for the cell height, spreading area, actin network arrangement and vinculin distribution at the cell-substrate interface. In line with the altered mechanical properties, we observed a functional increase in the cell migration rate and invasiveness. These alterations were significantly observed for NMuMG cells 48 h after tEMT.

The mechanical properties for various differentiating cell types should be prospectively defined to determine their future applications in medicine. In addition, the contribution of chemical factors and the TGF-β1-induced mechanical properties to cell alteration should be identified, and regulating mechanisms should be also clarified. In this study, we selected a typical epithelial cell EMT model; however, a primary cancer EMT model will be more suitable for future studies. The interpretation was still limited by only focus on two mechanical properties, stiffness and adhesion force.

Acknowledgments The authors acknowledge financial support from the National Science Council of Taiwan (98-2627-B-006-009-, 99-2627-B-006-009-, 100-2627-B-006-009-).

References

A. Albini, Y. Iwamoto, H.K. Kleinman, G.R. Martin, S.A. Aaronson, J.M. Kozlowski, R.N. McEwan, Cancer Res. **47**, 3239 (1987)
R.C. Bates et al., J. Clin. Investig. **115**, 339 (2005)
J.R. Beach et al., Proc. Natl. Acad. Sci. U. S. A. **108**, 17991 (2011)
W. Birchmeier, EMBO Rep. **6**, 413 (2005)
M.A. Brown, C.S. Wallace, C.C. Anamelechi, E. Clermont, W.M. Reichert, G.A. Truskey, Biomaterials **28**, 3928 (2007)
S.T. Buckley, C. Medina, A.M. Davies, C. Ehrhardt, Nanomedicine **8**, 355 (2012)
D. Buergy, F. Wenz, C. Groden, M.A. Brockmann, Int. J. Cancer **130**, 2747 (2012)
E. Canetta, A. Duperray, A. Leyrat, C. Verdier, Biorheology **42**, 321 (2005)
O. Chaudhuri, S.H. Parekh, W.A. Lam, D.A. Fletcher, Nat. Methods **6**, 383 (2009)
J. Chen, H. Li, N. SundarRaj, J.H. Wang, Cell Motil. Cytoskeleton **64**, 248 (2007)
C.-C. Chen, P.C.-H. Hsieh, G.-M. Wang, W.-C. Chen, M.-L. Yeh, Mater. Let. **63**, 1872 (2009)
Y.S. Chu, W.A. Thomas, O. Eder, F. Pincet, E. Perez, J.P. Thiery, S. Dufour, J. Cell Biol. **167**, 1183 (2004)
M.J. Colbert, F. Brochard-Wyart, C. Fradin, K. Dalnoki-Veress, Biophys. J. **99**, 3555 (2010)
S.E. Cross, Y.S. Jin, J. Tondre, R. Wong, J. Rao, J.K. Gimzewski, Nanotechnology **19**, 384003 (2008)
S.E. Cross, Y.S. Jin, Q.Y. Lu, J. Rao, J.K. Gimzewski, Nanotechnology **22**, 215101 (2011)
N. Desprat, A. Guiroy, A. Asnacios, Rev. Sci. Instrum. **77**, 055111 (2006)
D. Docheva, D. Padula, M. Schieker, H. Clausen-Schaumann, Biochem. Biophys. Res. Commun. **402**, 361 (2010)
A.J. Engler, S. Sen, H.L. Sweeney, D.E. Discher, Cell **126**, 677 (2006)
J. Friedrichs et al., J. Biol. Chem. **282**, 29375 (2007)
J. Friedrichs, J. Helenius, D.J. Muller, Nat. Protoc. **5**, 1353 (2010a)
J. Friedrichs, J. Helenius, D.J. Muller, Proteomics **10**, 1455 (2010b)
J. Friedrichs, A. Zieris, S. Prokoph, C. Werner, Macromol. Rapid Commun. **33**, 1453 (2012)
J. Friedrichs, K.R. Legate, R. Schubert, M. Bharadwaj, C. Werner, D.J. Muller, M. Benoit, Methods **60**, 169 (2013a)
J. Friedrichs, C. Werner, D.J. Muller, Methods Mol. Biol. **1046**, 19 (2013b)
A. Fuhrmann, J.R. Staunton, V. Nandakumar, N. Banyai, P.C. Davies, R. Ros, Phys. Biol. **8**, 015007 (2011)
N.D. Gallant, K.E. Michael, A.J. Garcia, Mol. Biol. Cell **16**, 4329 (2005)
S. Giampieri, C. Manning, S. Hooper, L. Jones, C.S. Hill, E. Sahai, Nat. Cell Biol. **11**, 1287 (2009)
F. Guilak, V.C. Mow, J. Biomech. **33**, 1663 (2000)
T. Itabashi et al., Nat. Methods **6**, 167 (2009)
A. Kabashima et al., Int. J. Cancer **124**, 2771 (2009)
D.H. Kim, S.B. Khatau, Y. Feng, S. Walcott, S.X. Sun, G.D. Longmore, D. Wirtz, Sci. Rep. **2**, 555 (2012)
M. Labelle, S. Begum, R.O. Hynes, Cancer Cell **20**, 576 (2011)
W.A. Lam, M.J. Rosenbluth, D.A. Fletcher, Br. J. Haematol. **142**, 497 (2008)
J. Lee, M. Leonard, T. Oliver, A. Ishihara, K. Jacobson, J. Cell Biol. **127**, 1957 (1994)
M.J. Lee, J. Kim, K.I. Lee, J.M. Shin, J.I. Chae, H.M. Chung, Cytotherapy **13**, 165 (2011)
M. Lekka, P. Laidler, Nat. Nanotechnol. **4**, 72 (2009). author reply 72
F. Li, S.D. Redick, H.P. Erickson, V.T. Moy, Biophys. J. **84**, 1252 (2003)
M.M. Lotz, C.A. Burdsal, H.P. Erickson, D.R. McClay, J. Cell Biol. **109**, 1795 (1989)
S.A. Mani et al., Cell **133**, 704 (2008)
J.C. Martens, M. Radmacher, Pflugers Arch. - Eur. J. Physiol. **456**, 95 (2008)
T.S. Matsui, S. Deguchi, N. Sakamoto, T. Ohashi, M. Sato, Biorheology **46**, 401 (2009)
P.J. Miettinen, R. Ebner, A.R. Lopez, R. Derynck, J. Cell Biol. **127**(6 Pt 2), 2021 (1994)
D. Mitrossilis, J. Fouchard, A. Guiroy, N. Desprat, N. Rodriguez, B. Fabry, A. Asnacios, Proc. Natl. Acad. Sci. U. S. A. **106**, 18243 (2009)
D. Mitrossilis, J. Fouchard, D. Pereira, F. Postic, A. Richert, M. Saint-Jean, A. Asnacios, Proc. Natl. Acad. Sci. U. S. A. **107**, 16518 (2010)
M. Mori et al., Mol. Biol. Cell **20**, 3115 (2009)
K. Nagayama, S. Yanagihara, T. Matsumoto, Med. Eng. Phys. **29**, 620 (2007)
R.M. Nerem, Adv. Exp. Med. Biol. **534**, 1 (2003)
G. Ofek, D.C. Wiltz, K.A. Athanasiou, Biophys. J. **97**, 1873 (2009)
C. Rotsch, M. Radmacher, Biophys. J. **78**, 520 (2000)
A. Saterbak, D.A. Lauffenburger, Biotechnol. Prog. **12**, 682 (1996)
S. Sen, S. Kumar, Cell. Mol. Bioeng. **2**, 218 (2009)
Y. Shen, M. Nakajima, S. Kojima, M. Homma, T. Fukuda, Biochem. Biophys. Res. Commun. **409**, 160 (2011)
J. Solon, I. Levental, K. Sengupta, P.C. Georges, P.A. Janmey, Biophys. J. **93**, 4453 (2007)
D.A. Starr, M. Han, J. Cell Sci. **116**, 211 (2003)
M.P. Stewart, J. Helenius, Y. Toyoda, S.P. Ramanathan, D.J. Muller, A.A. Hyman, Nature **469**, 226 (2011)

S. Suresh, Nat. Nanotechnol. **2**, 748 (2007)
V. Swaminathan, K. Mythreye, E.T. O'Brien, A. Berchuck, G.C. Blobe, R. Superfine, Cancer Res. **71**, 5075 (2011)
A. Taubenberger, D.A. Cisneros, J. Friedrichs, P.H. Puech, D.J. Muller, C.M. Franz, Mol. Biol. Cell **18**, 1634 (2007)
A.V. Taubenberger, D.W. Hutmacher, D.J. Muller, Tissue Eng. B Rev. **20**, 40 (2014)
G. Thoelking, B. Reiss, J. Wegener, H. Oberleithner, H. Pavenstaedt, C. Riethmuller, Nanotechnology **21**, 265102 (2010)
O. Thoumine, A. Ott, D. Louvard, Cell Motil. Cytoskeleton **33**, 276 (1996)
Q. Tseng et al., Lab Chip **11**, 2231 (2011)
C.E. Turner, J.R. Glenney Jr., K. Burridge, J. Cell Biol. **111**, 1059 (1990)
S. Vichare, M.M. Inamdar, S. Sen, Soft Matter, (2012a).
S. Vichare, M.M. Inamdar, S. Sen, Soft Matter **8**, 10464 (2012b)
X. Wang, S. Cooper, Tissue Eng. A **19**, 1113 (2012)
N. Wang, I.M. Tolic-Norrelykke, J. Chen, S.M. Mijailovich, J.P. Butler, J.J. Fredberg, D. Stamenovic, Am. J. Physiol. Cell Physiol. **282**, C606 (2002)
N. Wang, J.D. Tytell, D.E. Ingber, Nat. Rev. Mol. Cell Biol. **10**, 75 (2009)
C.C. Wu, H.W. Su, C.C. Lee, M.J. Tang, F.C. Su, Biochem. Biophys. Res. Commun. **329**, 256 (2005)
T.-H. Wu, C.-H. Li, M.-J. Tang, J.-I. Liang, C.-H. Chen, M.-L. Yeh, Cell Commun. Adhes. **20,** 115 (2013).
J. Zavadil, E.P. Bottinger, Oncogene **24**, 5764 (2005)
J. Zavadil et al., Proc. Natl. Acad. Sci. U. S. A. **98**, 6686 (2001)